catalysts

MDPI

Article

Advancing Sustainable Aviation: Bimetallic Co-Mo Catalysts for Bio-Jet Fuel Production from Sunflower and Waste Cooking Oils

Karoline K. Ferreira, Lucília S. Ribeiro * and Manuel Fernando R. Pereira

LSRE-LCM, ALiCE, Faculty of Engineering, University of Porto, Rua Dr. Roberto Frias, 4200-465 Porto, Portugal; up202103294@edu.fe.up.pt (K.K.F.); fpereira@fe.up.pt (M.F.R.P.)
* Correspondence: lucilia@fe.up.pt

Abstract

Co and Mo mono- and bimetallic catalysts supported on CNT-H-ZSM-5 composites were prepared and characterized using various techniques. The catalysts were evaluated for the conversion of sunflower oil (SO) into sustainable aviation fuel (SAF) hydrocarbons in the C_8–C_{16} range. The effects of reduction temperature and metal loading were the main parameters investigated in this study. The catalyst reduced at 600 °C promoted the formation of Mo_2C species, resulting in high SO conversion (84%), complete deoxygenation, and enhanced isomerization within the C_8–C_{16} fraction. Optimal metal loadings (2.5 wt% Co and 8 wt% Mo) and the bimetallic configuration led to superior performance compared with monometallic catalysts and physical mixtures, clearly highlighting a synergistic effect between Co and Mo species. In contrast, when waste cooking oil was used as feedstock, lower conversion and reduced selectivity toward SAF-range hydrocarbons were observed, which were attributed to the higher complexity and impurity content of this residue feedstock.

Keywords: bio-jet fuel; cracking and isomerization; triglycerides deoxygenation; carbon nanotubes; zeolite; Co and Mo catalysts

1. Introduction

The transportation sector has focused its energy transition efforts on the development of bio-based fuels. Aviation, in particular, has significantly increased its activity in both passenger and cargo transport [1]. As a result, the rise in greenhouse gas (GHG) emissions has raised concerns among regulatory institutions due to the impact of these gases on the worsening of the climate crisis in recent years [2]. In response to this scenario, the International Air Transport Association has established targets to decarbonize the aviation sector by 2050, including the development of new aircraft engine technologies, carbon capture, and the use of sustainable aviation fuel (SAF) [3,4]. Among these strategies, SAF is considered the most promising option for reducing GHG emissions, as it relies on renewable feedstocks and contributes to closing the carbon cycle [5].

SAF consists of hydrocarbons in the C_8 to C_{16} carbon range, with a predominance of alkanes. One of the most important aspects is that the content of isomers must be higher than that of *n*-alkanes in order to ensure the cold properties required by fuel standards [6,7]. For the production of SAF, several technological routes enable the conversion of different feedstocks into this biofuel [8,9]. Among them, the hydroprocessing of esters and fatty acids (HEFA) stands out as one of the most strategic routes for the short-term deployment of SAF [10]. In this process, lipid-based feedstocks, such as vegetable oils and waste cooking

Check for updates

Academic Editors: Ivan V. Kozhevnikov, Eliana Sousa Da Silva and Katarzyna Morawa Eblagon

Received: 24 February 2026
Revised: 11 March 2026
Accepted: 14 April 2026
Published: 1 May 2026

Copyright: © 2026 by the authors. Licensee MDPI, Basel, Switzerland. This article is an open access article distributed under the terms and conditions of the Creative Commons Attribution (CC BY) license.

oil (WCO), undergo multiple hydroprocessing steps to produce liquid fuels within the desired hydrocarbon range [11]. The high oxygen content of these feedstocks reduces fuel combustion efficiency and negatively affects chemical stability, while increasing viscosity, acidity, and corrosiveness, which pose challenges for storage and transportation [12]. Therefore, in addition to oil deoxygenation, cracking and isomerization reactions are required to enhance selectivity toward jet fuel fractions and to increase the yield of isomers within the target range [13].

Several catalytic systems have been investigated for the conversion of lipid-based feedstocks into SAF. The main challenge is to increase selectivity within the C_8–C_{16} range while avoiding excessive cracking to lighter fractions, such as gasoline and gases [14]. Consequently, studies addressing this issue have gained increasing attention in the literature in recent years. The development of supported bifunctional catalysts is of great importance, as it enables triglyceride deoxygenation as well as the cracking and isomerization reactions required [15–19]. In this context, a class of catalysts has emerged for the conversion of vegetable oils and WCO. Non-noble transition metals, including Co, Mo, Fe, and Ni, are widely used in hydrotreating reactions of both petrochemical and renewable feedstocks [20]. Furthermore, supports such as Al_2O_3, SiO_2, mesoporous silicas, and zeolites are commonly employed in the aforementioned reactions [21].

Zeolites are aluminosilicates composed of corner-sharing TO_4 tetrahedra, in which T typically represents silicon and aluminum. The isomorphic substitution of Si^{4+} by Al^{3+} within the crystalline framework generates negative charges that, when compensated by protons, give rise to Brønsted acid sites [22]. In their protonic form (H^+-zeolites), these materials exhibit tunable acid–base properties, making them particularly suitable for catalytic reactions such as cracking and isomerization [23]. However, zeolites are predominantly microporous materials, which hampers the diffusion of bulky molecules, such as triglycerides present in vegetable oils and lipid residues, into the internal pore structure. This intraparticle diffusion limitation leads to low yields of desired products and promotes excessive coke formation, mainly due to the high acidity of the material [21,24].

In contrast, mesoporous carbon materials, such as carbon nanotubes (CNTs), display favorable physicochemical properties for the conversion of lipid sources into liquid fuels. The absence of micropores, combined with high mechanical and thermal stability and large pore volume, makes CNTs suitable supports for the metallic phase in deoxygenation reactions [25]. Additionally, CNT-based materials exhibit remarkable stability after consecutive reaction cycles under severe temperature and pressure conditions [26–28]. Nevertheless, previous studies have reported the limited cracking and isomerization capacity of CNT-based catalysts [27,29].

Previous works have shown that Co-Mo/CNT catalysts physically mixed with H-ZSM-5 zeolite exhibit high catalytic activity toward the production of lighter hydrocarbon fractions (C_5–C_{16}) from WCO, although accompanied by excessive cracking [30]. On the other hand, Co–Mo catalysts supported on CNT–H-ZSM-5 composite materials were investigated in our previous work for the conversion of a model compound (palmitic acid), yielding highly promising results for the aviation fuel range, with approximately 34% selectivity toward C_8–C_{16} hydrocarbons [31]. These findings highlight the synergistic potential of CNTs and H-ZSM-5 for the conversion of oils into hydrocarbons suitable for SAF production.

To the best of our knowledge, no detailed study has yet addressed the optimization of the metallic phase in CNT–H-ZSM-5 composite catalysts applied to the conversion of real lipid feedstocks, such as sunflower oil and WCO. Based on our prior study on Co–Mo/CNT–H-ZSM-5 (2.5 wt% Co and 10.5 wt% Mo) catalysts [31], the present work further explores this catalytic system using real lipid feedstocks. In this work, the influence

of the metallic phase on catalytic performance and product distribution was thoroughly investigated, aiming to enhance hydrocarbon yields within the SAF range while mitigating excessive cracking and coke formation. This approach provides relevant insights into the design of bifunctional composite catalysts for the efficient upgrading of renewable lipid sources into drop-in fuels.

2. Results and Discussion

2.1. Catalysts' Characterization

To investigate the reduction behavior of the 2.5Co10.5Mo catalyst, H_2-TPR analyses were performed on the N_2-treated catalysts (without prior reduction). For comparison, the monometallic 10.5Mo catalyst was also analyzed. As shown in Figure 1, the 10.5Mo catalyst exhibits a broad hydrogen consumption peak between 400 and 600 °C, which is assigned to the reduction of Mo^{6+} to Mo^{4+} [28,32]. In addition, a high temperature peak centered at approximately 700 °C is observed and attributed to the further reduction of Mo^{4+} to Mo^0 [32]. In the case of the bimetallic 2.5Co10.5Mo catalyst, an increased hydrogen consumption is observed in the 400–600 °C temperature range, indicating a clear promoter effect of Co on the reducibility of Mo species.

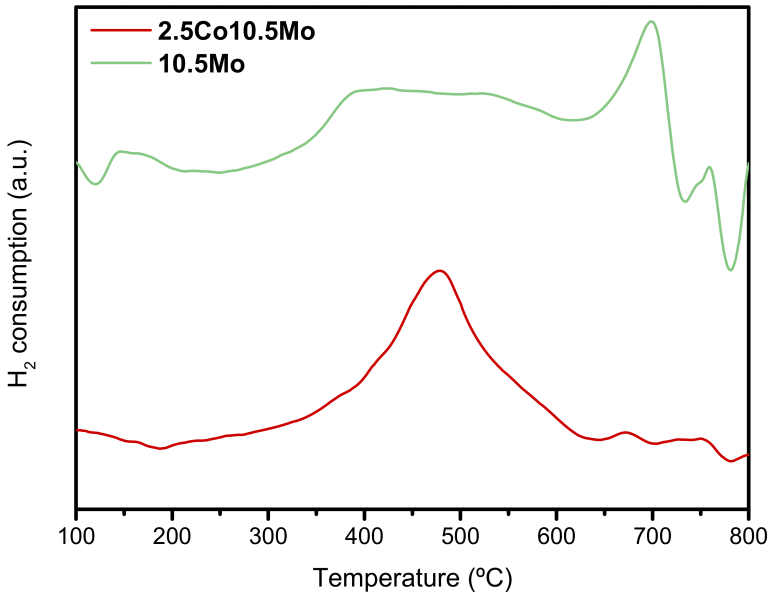


Figure 1. H_2-TPR of 10.5Mo and 2.5Co10.5Mo supported catalyst (N_2-treated).

Subsequently, selected catalysts were analyzed by XRD. Initially, the 2.5Co10.5Mo catalysts reduced at different temperatures (500, 550, and 600 °C) were investigated to evaluate the evolution of the metallic phases. As shown in Figure 2, all catalysts exhibit the characteristic crystalline phases of H-ZSM-5, as well as the (011) graphite plane of CNTs at 2θ = 26°, which overlaps with the (011) monoclinic MoO_2, as reported elsewhere [31]. Additional diffraction peaks associated with MoO_2 are observed at 2θ = 37° and 53°, corresponding to the (020) and (022) planes, respectively (PDF #00-032-0671). No diffraction peaks associated with Co species were detected, which is most likely related to its low loading in the catalysts (around 2 wt%), as further confirmed by ICP-OES analysis. In addition, TEM results presented below indicate similar dispersion for both Co and Mo particles, suggesting that the absence of detectable Co crystalline phases is mainly due to its lower content rather than differences in dispersion.

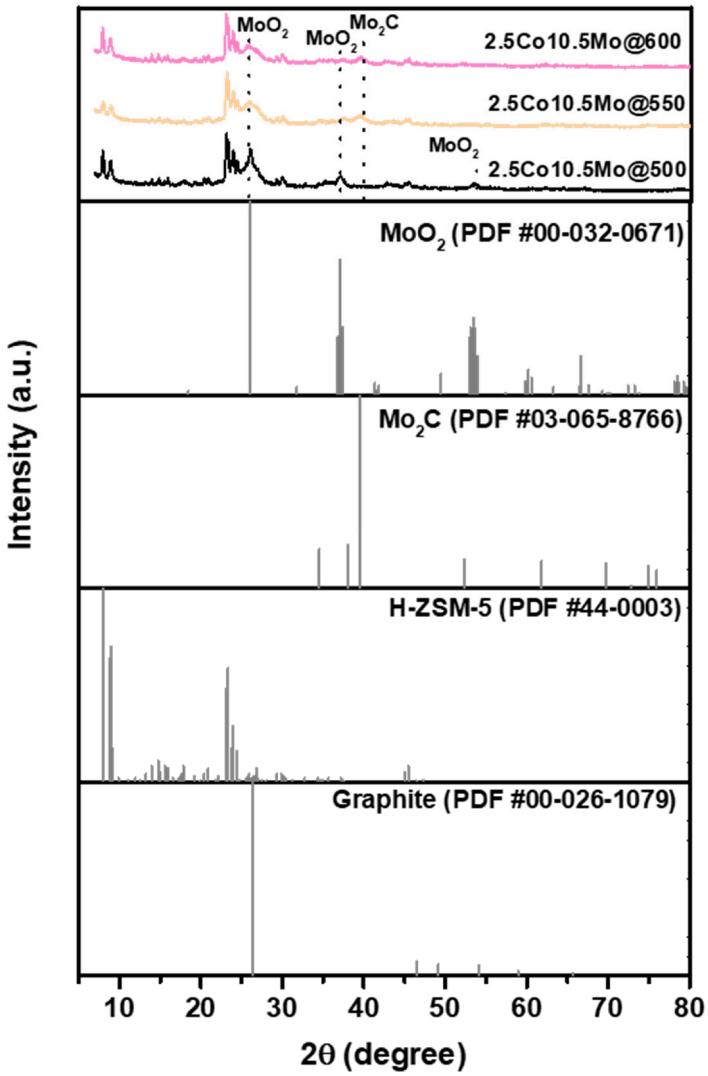


Figure 2. XRD patterns of 2.5Co10.5Mo catalysts reduced at 500, 550 and 600 °C.

It is observed that, as the reduction temperature increases, the intensity of the MoO_2 reflections decreases, while the formation of Mo_2C becomes evident at 2θ = 39° (PDF #03-065-8766). The presence of Mo_2C phases has been widely reported for Mo-based catalysts supported on carbon materials such as CNTs and carbon nanofibers [28,33]. According to Wang et al. [34], the formation of Mo_2C follows a reduction-carburization pathway ($MoO_3 \rightarrow MoO_2 \rightarrow Mo_2C$) under a hydrogen atmosphere. The same authors also reported that, at temperatures below 1070 °C, the coexistence of MoO_2, Mo_2C, and metallic Mo phases is commonly observed.

The textural properties of the support and metal-loaded catalysts were determined by N_2 adsorption isotherms and are summarized in Table 1. The CNHZ support exhibits a high specific surface area (S_{BET} = 267 m^2 g_{cat}^{-1}) and a large total pore volume (V_{pore} = 1.16 cm^3 g_{cat}^{-1}), which are essential features for promoting good dispersion of the metallic phases on the support surface. In addition, CNHZ presents a high external surface area (S_{ext} = 217 m^2 g_{cat}^{-1}) and a low micropore volume, indicating that the mesoporosity of the CNT component is preserved, while the zeolite component still contributes to the overall textural properties of the composite material.

Table 1. Textural properties of the CNHZ support and catalysts.

Sample	$S_{BET} \pm 20$ ($m^2\ g_{cat}^{-1}$)	$S_{ext} \pm 10$ ($m^2\ g_{cat}^{-1}$)	$V_{micro} \pm 0.01$ ($cm^3\ g_{cat}^{-1}$)	$V_{pore} \pm 0.04$ ($cm^3\ g_{cat}^{-1}$)	V_{micro}/V_{pore}
CNT [a]	229	229	0.00	1.54	0.00
H-ZSM-5 [a]	352	62	0.13	0.21	0.62
CNHZ	267	217	0.03	1.16	0.03
2.5Co10.5Mo_500	217	140	0.04	0.76	0.05
2.5Co10.5Mo_550	234	163	0.03	0.83	0.04
2.5Co10.5Mo_600	249	180	0.03	1.03	0.03
2.5Co	294	142	0.06	0.40	0.15
8Mo	250	199	0.03	0.91	0.03
2.5Co8Mo	247	177	0.03	1.09	0.03
2.5Co13Mo	212	135	0.04	0.97	0.04
1Co8Mo	230	164	0.03	1.05	0.03
4Co8Mo	248	175	0.04	0.75	0.05

[a] Values reported by Ferreira et al. [31].

For both mono- and bimetallic catalysts, a decrease in specific surface area and total pore volume is observed relative to the support. This behavior is consistent with the introduction of metallic phases, which partially block the pores and reduce the accessible surface area. The extent of this decrease correlates with the total metal loading, which ranges from 9 to 15.5 wt% for the bimetallic catalysts and from 2.5 to 8 wt% for the monometallic catalysts.

In contrast, the monometallic catalyst 2.5Co exhibits a significantly higher S_{BET} value (294 $m^2\ g_{cat}^{-1}$) compared with the support and the other catalysts. The textural analysis also reveals a pronounced increase in the relative contribution of micropores, with a V_{micro}/V_{pore} ratio of 0.15, indicating a substantial shift toward microporous character. These features suggest that the presence of Co alone may promote a different interaction with the carbon phase, possibly leading to partial decomposition or restructuring of CNTs during thermal treatments (500 °C under N_2 and 600 °C under H_2). As a consequence, the mesoporous contribution associated with the carbon phase is reduced, while the intrinsic microporosity of H-ZSM-5 becomes more predominant. This redistribution of the support components explains the simultaneous increase in S_{BET} and the rise in the V_{micro}/V_{pore} ratio observed for the 2.5Co catalyst.

Isotherms of the materials are presented in Figure S1. According to the results, all catalysts exhibited type II isotherms [27], characteristic of mesoporous materials. Moreover, these results are consistent with those reported in our previous work using the same catalyst support [31].

The Co and Mo metal loadings of the catalysts were determined by ICP-OES and are summarized in Table 2. Overall, the experimental metal contents are in good agreement with the nominal values, considering the associated experimental uncertainty. Slight deviations between the nominal and measured loadings were observed, which can be attributed to metal losses during impregnation, drying, and reduction steps, as well as to differences in metal-support interactions. Nevertheless, these results confirm that the targeted Co and Mo loadings were successfully achieved for both mono- and bimetallic catalysts.

On the other hand, the monometallic 2.5Co catalyst presented a higher Co content (4.3 wt%) than the nominal value of 2.5 wt%. This discrepancy is consistent with the textural properties discussed above and can be attributed to a partial loss of the carbon phase during the thermal treatment and reduction steps, which leads to an apparent

increase in the measured metal concentration. In contrast, the presence of Mo in the bimetallic catalysts appears to enhance the thermal stability of the CNT-HZSM-5 support.

To investigate the dispersion of Co and Mo nanoparticles, HAADF-STEM analysis was performed on selected catalysts (Figure 3). In general, both metal phases are well dispersed over the support in all samples. However, the 1Co8Mo catalyst (Figure 3A), which has a lower metal loading, exhibits a higher degree of particle dispersion over the CNHZ composite. In contrast, catalysts with higher metal contents, such as 2.5Co8Mo (Figure 3B) and 2.5Co13Mo (Figure 3C), show evidence of particle agglomeration. Additionally, some Co and Mo species appear to be spatially associated, suggesting the possible formation of bimetallic domains.

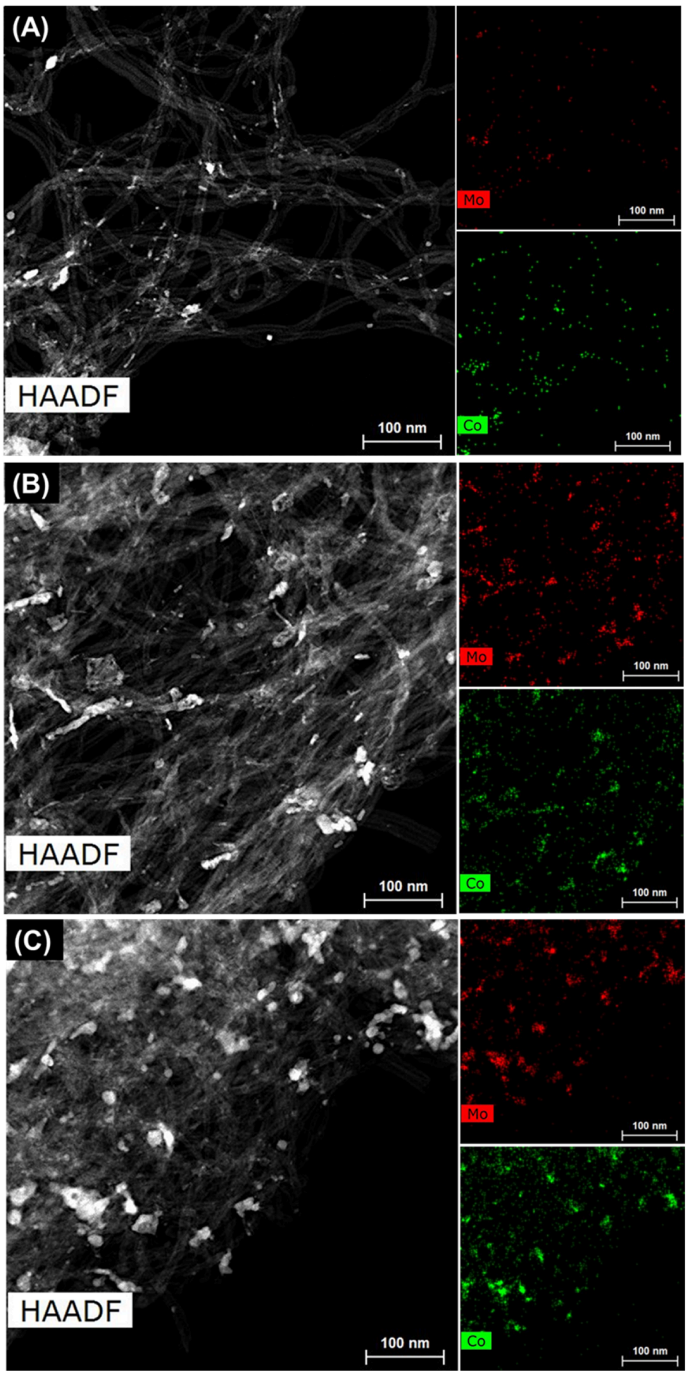


Figure 3. HAADF-STEM images of (**A**) 1Co8Mo, (**B**) 2.5Co8Mo and (**C**) 2.5Co13Mo.

Table 2. Metal loading of the mono- and bimetallic catalysts.

Sample	Co ± 0.2 (%)	Mo ± 0.4 (%)
2.5Co10.5Mo_500	1.6	9.1
2.5Co10.5Mo_550	1.8	9.9
2.5Co10.5Mo_600	1.9	10.6
2.5Co	4.3	-
8Mo	-	8.1
2.5Co8Mo	2.1	9.4
2.5Co13Mo	2.1	13.5
1Co8Mo	0.8	8.6
4Co8Mo	3.7	7.0

2.2. SO and WCO Characterization Results

Based on the results presented in Table S1, the fatty acid composition of WCO was compared with the typical profile reported for SO. While SO is characterized by a high content of polyunsaturated fatty acids, particularly linoleic acid (C18:2), ranging from 45.0 to 74.0 wt%, the WCO sample exhibited a significantly lower proportion of this component (25.1 wt%). In contrast, WCO showed a much higher content of oleic acid (C18:1), reaching 61.1 wt%, whereas SO typically ranges from 14.0 to 43.0 wt%. Saturated fatty acids such as palmitic acid (C16:0) and stearic acid (C18:0) were present in similar proportions in both oils, although WCO exhibited a slightly higher palmitic acid content (8.8 wt%). Minor fatty acids, including long-chain saturated compounds (C20:0–C24:0), were detected only in small amounts, indicating that both feedstocks are predominantly composed of C_{16} and C_{18} fatty acids.

Overall, the higher oleic acid content and lower degree of polyunsaturation observed in WCO may be attributed to thermal and oxidative degradation processes occurring during repeated cooking cycles [35].

2.3. Catalytic Reactions Results

The catalysts were evaluated for the conversion of SO into liquid and gaseous products. Initially, catalysts reduced at different temperatures were investigated. As shown in Table 3, the reduction temperature plays a crucial role in both conversion and product selectivity. The catalyst reduced at 500 °C (2.5Co10.5Mo_500) exhibited the lowest conversion (36%), with the formation of intermediate oxygenated compounds resulting from incomplete deoxygenation reactions and a low iso/*n* ratio (0.2) in the C_8–C_{16} fraction.

Table 3. Catalytic performance of Co–Mo catalysts reduced at different temperatures.

Catalyst	Selectivity (%)					Conversion (%)	iso/*n* (C_8–C_{16})
	C_1–C_4	C_5–C_7	C_8–C_{16}	C_{17}–C_{24}	Oxygenated Compounds		
2.5Co10.5Mo_500	1	5	46	39	9	36	0.2
2.5Co10.5Mo_550	8	4	54	34	0	41	0.6
2.5Co10.5Mo_600	16	15	43	26	0	84	1.9

Reaction conditions: 325 °C, 20 bar initial H_2 pressure (at room temperature), 0.5 g of SO in 50 mL of *n*-decane, 0.1 g of catalyst, 300 rpm, and 3 h of reaction.

When the reduction temperature was increased to 550 °C, complete deoxygenation of oxygenated intermediates into alkanes was achieved, accompanied by an increased formation of gaseous products (C_1–C_4). This effect became more pronounced for the catalyst reduced at 600 °C (2.5Co10.5Mo_600), which showed a significantly higher conversion (84%) and increased selectivity toward lighter alkanes (21% in the C_1–C_7 range). In addition,

a higher degree of isomerization was observed, as evidenced by the increased iso/*n* ratio (1.9) in the C_8–C_{16} fraction.

Although CO and CO_2 were not analyzed in this work, a previous study with similar Co-Mo/CNT catalysts under comparable conditions has shown that deoxygenation of WCO mainly proceeds via the hydrodeoxygenation pathway due to the presence of MoO_2 species [27]. According to the same work, the major contribution to the gas products selectivity was related to methane and propane. The same trend was observed by Ribeiro et al. [30], who studied the conversion of Co-Mo/CNT and H-ZSM-5 in a continuous reactor under similar conditions. In this context, the contribution of CO and CO_2 for the conversion and selectivity is minimal.

As discussed in the XRD analysis, reduction at 600 °C favors the formation of the Mo_2C phase, which is known to exhibit higher catalytic activity than MoO_2 species in hydrogenation reactions [28,33]. Furthermore, cracking and isomerization reactions require the synergistic interaction between metallic and acidic sites, with close proximity being essential for efficient reaction pathways [36,37]. Therefore, the presence of Mo_2C species in close contact with the acidic sites of the zeolite within the composite catalyst enhances conversion to liquid and gaseous products and promotes isomerization in the C_8–C_{16} fraction. Based on these results, all subsequent catalysts were reduced at 600 °C.

Subsequently, the effect of Co and Mo metal loading was investigated. First, the influence of Mo addition was evaluated while keeping the Co loading constant at 2.5 wt% (Figure 4).

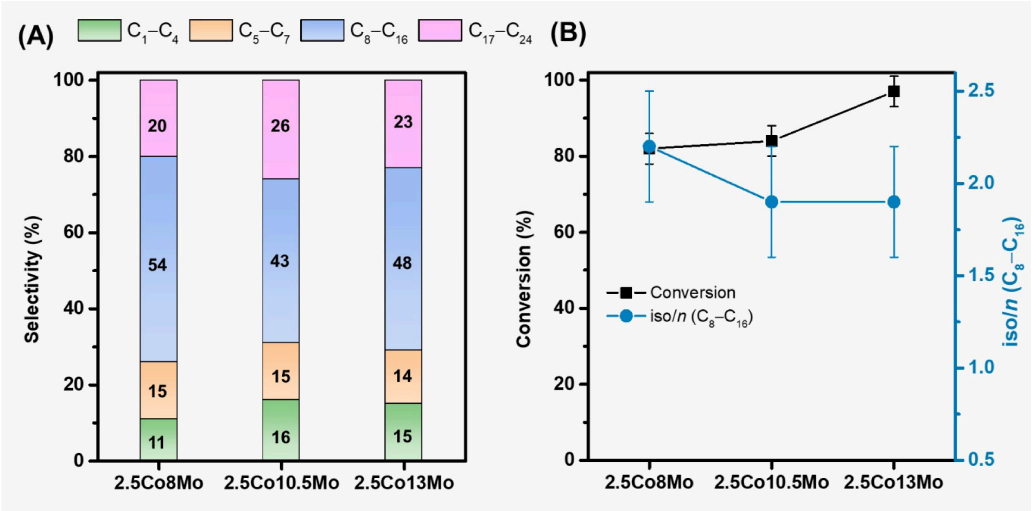


Figure 4. Effect of Mo loading on the catalytic performance of bimetallic Co-Mo catalysts: (**A**) product selectivity and (**B**) SO conversion and iso/*n* ratio in the C_8–C_{16} range. Reaction conditions: 325 °C, 20 bar initial H_2 pressure (at room temperature), 0.5 g of SO in 50 mL of *n*-decane, 0.1 g of catalyst, 300 rpm, and 3 h of reaction.

The analysis of product selectivity across different hydrocarbon ranges (Figure 4A) shows that increasing the Mo content from 8 to 10.5 wt% led to a slight increase in the selectivity toward heavier hydrocarbons (C_{17}–C_{24}), from 20% to 26%, accompanied by a decrease in the C_8–C_{16} fraction associated with SAF, from 54% to 43%. Further increasing the Mo loading to 13 wt% did not result in significant changes in selectivity toward light alkanes; however, a slight increase in the C_8–C_{16} fraction was observed.

Regarding SO conversion (Figure 4B), the 2.5Co13Mo catalyst exhibited a higher conversion, whereas the 2.5Co8Mo and 2.5Co10.5Mo catalysts showed similar conversion values. Overall, all the catalysts produced a similar iso/*n* ratio in the C_8–C_{16} range.

As reported elsewhere [27,30], the incorporation of metal species into supported catalysts increases the total acidity due to interactions between Co and Mo species and changes in surface charge distribution. Although the higher Mo loading (13 wt%) enhanced SO conversion, catalysts with higher Mo content slightly favored cracking reactions, leading to an increased formation of lighter hydrocarbons. Therefore, considering selectivity toward the C_8–C_{16} fraction, a Mo loading of 8 wt% was selected as the optimal composition.

Similarly, the effect of Co loading was evaluated while keeping the Mo content fixed at 8 wt% (Figure 5). As shown in Figure 5A, increasing the Co loading from 1 to 2.5 wt% led to a significant increase in the C_8–C_{16} fraction, accompanied by a decrease in heavier hydrocarbon fractions. The higher availability of metallic sites was crucial for enhancing selectivity toward the SAF range, which reached values of approximately 52–54% for the 2.5Co8Mo and 4Co8Mo catalysts.

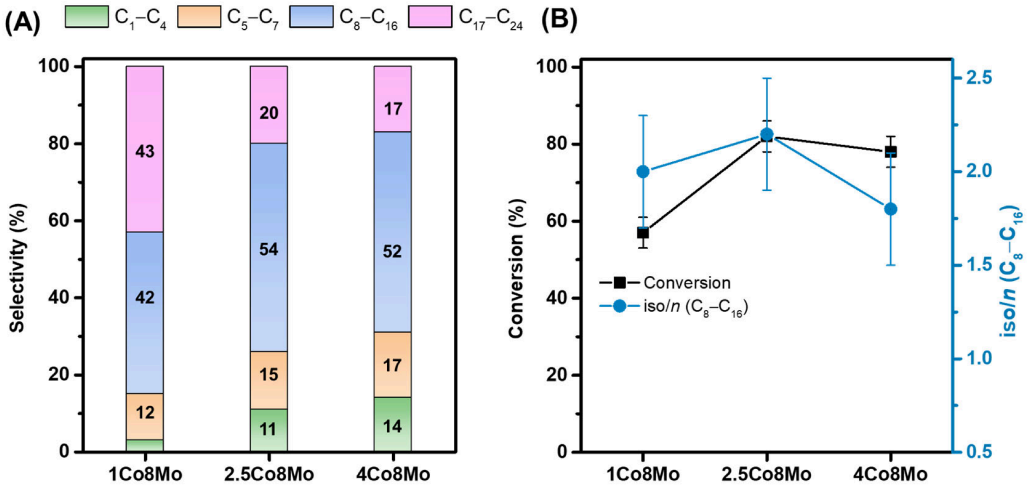


Figure 5. Effect of Co loading on the catalytic performance of bimetallic Co-Mo catalysts: (**A**) product selectivity and (**B**) SO conversion and iso/*n* ratio in the C_8–C_{16} range. Reaction conditions: 325 °C, 20 bar initial H_2 pressure (at room temperature), 0.5 g of SO in 50 mL of *n*-decane, 0.1 g of catalyst, 300 rpm, and 3 h of reaction.

A similar trend was observed for conversion and the iso/*n* ratio (Figure 5B). The conversion increased markedly from 57% to approximately 80% with increasing Co loading. In contrast, the iso/*n* ratio in the C_8–C_{16} range remained nearly constant, around 2.0, for all three catalysts, consistent with the behavior observed when varying the Mo content.

These results indicate that, under the investigated conditions, isomerization is more strongly associated with the acidic properties of the support rather than with the metallic phase. Based on these results, a Co loading of 2.5 wt% was selected for subsequent experiments.

To further elucidate the role of metal synergy, monometallic catalysts, a physical mixture of Co and Mo catalysts, and the corresponding bimetallic catalyst were evaluated under identical reaction conditions (Figure 6). As shown in Figure 6A, the monometallic catalysts exhibited high selectivity toward heavier hydrocarbon fractions, reaching 50% and 30% for the 2.5Co and 8Mo catalysts, respectively. In addition, the 2.5Co catalyst still produced intermediate oxygenated compounds, indicating incomplete deoxygenation.

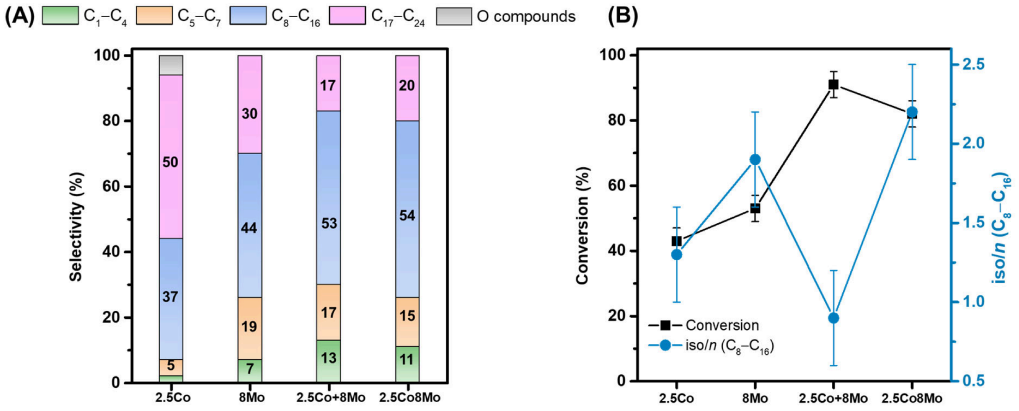


Figure 6. Comparison of monometallic, physical mixture, and bimetallic Co-Mo catalysts: (**A**) product selectivity and (**B**) conversion and iso/*n* ratio in the C_8–C_{16} range. Reaction conditions: 325 °C, 20 bar initial H_2 pressure (at room temperature), 0.5 g of SO in 50 mL of *n*-decane, 0.1 g of catalyst, 300 rpm, and 3 h of reaction.

Although the physical mixture displayed product selectivities similar to those of the bimetallic catalyst, significant differences were observed in terms of conversion and iso/*n* ratio (Figure 6B). The monometallic catalysts achieved moderate conversions, ranging from 43% to 53%, whereas the physical mixture reached a considerably higher conversion of approximately 90%. Despite this high conversion and comparable selectivity toward hydrocarbons in the SAF range, the iso/*n* ratio (C_8–C_{16}) was substantially higher for the bimetallic catalyst (2.2) than for the physical mixture (0.9).

These results clearly demonstrate that the superior catalytic performance of the bimetallic system cannot be achieved by simple physical mixing of the monometallic components. Instead, the intimate interaction between Co and Mo species in the bimetallic catalyst promotes a more efficient balance between hydrodeoxygenation, cracking, and isomerization reactions, leading to enhanced selectivity and improved fuel quality.

The recyclability of the catalyst was also assessed through three consecutive runs. After each cycle, the catalyst was recovered by filtration, thoroughly washed several times with acetone, and dried overnight at 110 °C prior to the next catalytic run. The results presented in Table 4 show a significant decline in catalytic activity from the second run onward. A marked decrease in conversion was observed, dropping from 82% in the first run to 70% and 76% in the second and third runs, respectively.

Table 4. Catalytic recyclability of 2.5Co8Mo in the conversion of SO.

Run	Selectivity (%)					Conversion (%)	iso/*n* (C_8–C_{16})
	C_1–C_4	C_5–C_7	C_8–C_{16}	C_{17}–C_{24}	Oxygenated Compounds		
1st	11	15	54	20	-	82	2.2
2nd	1	0	42	48	9	70	1.8
3rd	0	3	36	27	34	76	0.4
1st after regeneration [a]	7	9	55	29	-	100	2.4

[a] Regenerated after 1st run. Reaction conditions: 325 °C, 20 bar initial H_2 pressure (at room temperature), 0.5 g of SO in 50 mL of *n*-decane, 0.1 g of catalyst, 300 rpm, and 3 h of reaction.

In addition, selectivity toward the desired C_8–C_{16} fraction was considerably reduced, accompanied by an increased formation of oxygenated compounds, particularly in the third run (34%). This loss of catalytic performance may be attributed to the progressive deactivation of active sites, most likely caused by coke deposition. Similar behavior has

been reported elsewhere for the same catalyst under comparable reaction conditions during the conversion of palmitic acid [31].

To evaluate the possibility of restoring the catalyst activity, a regeneration treatment was carried out after the first run. The spent catalyst was calcined under air flow at 350 °C for 1 h to remove coke deposits, followed by a reduction step at 600 °C to ensure that the metallic particles remained in their reduced, active form. After regeneration, the catalyst exhibited complete recovery of conversion (100%), and the product's selectivity was very similar to that of the first run, indicating that catalyst deactivation is at least partially reversible and primarily related to coke deposition rather than irreversible structural damage.

Finally, the same catalyst was used to convert WCO into hydrocarbons, as shown in Table 5. The 2.5Co8Mo catalyst exhibited inferior catalytic activity for WCO conversion compared with SO. Under identical reaction conditions, only 63% of WCO was converted, with the highest selectivity observed toward heavier hydrocarbon fractions, reaching 56% in the C_{17}-C_{24} range, while only 30% of the products were distributed within the SAF-range (C_8–C_{16}).

Table 5. Catalytic performance of the 2.5Co8Mo catalyst in the conversion of different lipid substrates.

Substrate	Selectivity (%)					Conversion (%)	iso/*n* (C_8–C_{16})
	C_1–C_4	C_5–C_7	C_8–C_{16}	C_{17}–C_{24}	Oxygenated Compounds		
SO	11	15	54	20	-	82	2.2
WCO	1	5	30	56	8	63	0.5

Reaction conditions: 325 °C, 20 bar initial H_2 pressure (at room temperature), 0.5 g of SO in 50 mL of *n*-decane, 0.1 g of catalyst, 300 rpm, and 3 h of reaction.

A detailed analysis of the C_8–C_{16} fraction for both feedstocks (Figure 7) revealed significant differences in hydrocarbon composition. In the case of SO, the products consisted predominantly of iso-alkanes (38%), along with 16% of *n*-alkanes, indicating a more selective conversion pathway. In contrast, WCO resulted in a broader hydrocarbon distribution, with selectivities of 14% for *n*-alkanes, 8% for branched isomers, 7% for alkenes, and 1% for aromatic compounds.

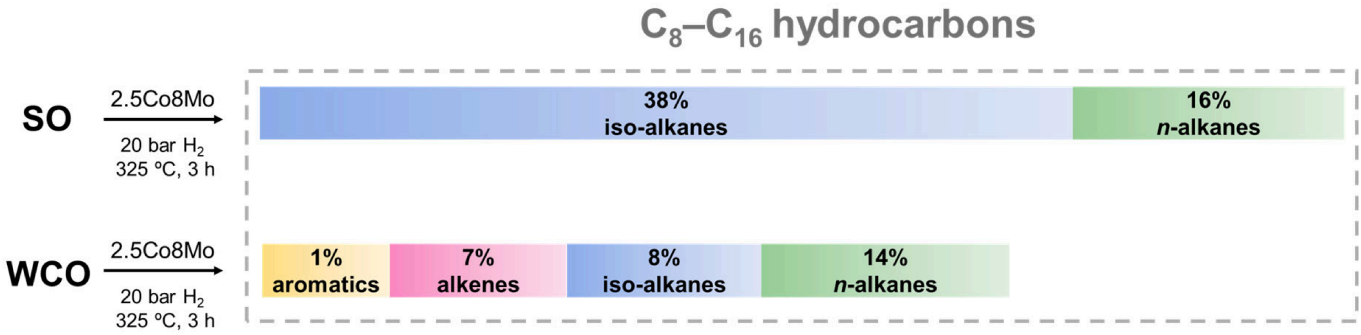


Figure 7. Composition of the C_8–C_{16} hydrocarbon fraction obtained from SO and WCO conversion over the 2.5Co8Mo.

Although the fatty acid profile of WCO shows a higher oleic acid (C18:1) content (61.1 wt%) compared to SO (maximum of 43 wt%), mechanistic studies on triglyceride conversion have demonstrated that, regardless of the initial fatty acid composition, unsaturated triglycerides are first hydrogenated to their corresponding saturated species before undergoing deoxygenation and cracking reactions [30,38]. Therefore, the superior performance of the 2.5Co8Mo catalyst in the conversion of SO is mainly attributed to the

higher purity of this refined commercial oil. In contrast, WCO is a considerably more complex feedstock, potentially containing residual water even after degumming, as well as phospholipids and other heteroatom-containing impurities. Such differences in feedstock composition can partially explain the lower conversion and reduced selectivity toward the desired SAF-range hydrocarbons observed for WCO.

3. Materials and Methods

3.1. Chemicals and Materials

Multiwalled carbon nanotubes (CNTs) (Nanocyl-7000, purity of 90%) and *n*-decane (99%) were provided by Nanocyl (Sambreville, Belgium) and VWR (Radnor, PA, USA), respectively. The metal precursors ammonium heptamolybdate (99.7%) and cobalt (II) nitrate hexahydrate (99%) were purchased from Riedel-de Han (Seelze, Germany) and Sigma-Aldrich (Darmstadt, Germany), respectively. Ammonium type ZSM-5 (SiO_2:Al_2O_3 mole ratio 30:1) was purchased from Alfa Aesar (Waltham, MA, USA). Sunflower oil (SO) was acquired from Fula (Sovena Group; Algés, Portugal), while WCO was kindly supplied by the Instituto of Carboquímica—ICB (Zaragoza, Spain).

3.2. Support Preparation

First, ammonium-type ZSM-5 (NH_4-ZSM-5) was calcined at 600 °C in air for 3 h to obtain its acid form (H-ZSM-5). A physical mixture between pristine CNT and H-ZSM-5 (2:1 weight ratio) was put into a ball-mill modelRetsch Mixer Mill MM 200 (Retsch GmbH, Haan, Germany) using two zirconium dioxide balls and a grinding jar. The two materials were milled for 60 min at 10 vibrations s^{-1}, producing a composite labeled as CNHZ.

3.3. Catalyst Preparation

Co (2.5 wt%) and Mo (10.5 wt%) were impregnated onto the support by the incipient wetness impregnation method, dried overnight at 110 °C, and subsequently thermally treated in a tubular furnace under an N_2 flow of 100 cm^3 min^{-1} for 3 h at 500 °C. The samples were then reduced under an H_2 flow of 100 cm^3 min^{-1} for 3 h at temperatures ranging from 500 to 600 °C, yielding the 2.5Co10.5Mo_X catalysts, where X denotes the reduction temperature. Afterwards, the samples were passivated under a 1% O_2/N_2 flow of 100 cm^3 min^{-1} for 1 h at room temperature. The same procedure was applied for another series of bimetallic supported catalysts with different Co (1 and 4 wt%) and Mo (8 and 13 wt%) loadings, using the optimal reduction temperature identified in the previous step. This procedure yielded the *z*Co*w*Mo catalysts, where *z* and *w* denote the Co and Mo loadings, respectively. The same protocol was also applied to monometallic catalysts, selecting the most promising Co and Mo loadings.

3.4. Catalyst Characterization

Hydrogen temperature programmed reduction (H_2-TPR) was performed using an AMI-300 equipment (Altamira Instruments, Pittsburgh, PA, USA). The N_2-treated catalyst was first held at 50 °C for 1 h under a 5% (*v*/*v*) H_2/Ar flow (total flow rate of 30 cm^3 min^{-1}). Subsequently, the temperature was increased to 900 °C at a heating rate of 10 °C min^{-1} under the same gas atmosphere.

X-ray diffraction (XRD) patterns of the catalysts were recorded using a Philips X'Pert MPD (Malvern Panalytical, Almelo, The Netherlands) diffractometer equipped with Cu Kα radiation (λ = 0.15406 nm). The diffraction intensities were measured over a 2θ range of 5° to 80° to analyze the crystalline structure of the samples.

Textural properties of the support and catalysts were evaluated by N_2 adsorption isotherms at −196 °C using a Quantachrome NOVA 4200e Surface Area and Pore Size analyzer (Anton Paar GmbH, Graz, Austria). The total specific surface area was determined by the Brunauer–Emmett–Teller (BET) method (S_{BET}), while the external surface area (S_{ext}) and micropore volume (V_{micro}) were obtained from the *t*-plot method. The total pore volume (V_{pore}) was calculated from the amount of N_2 adsorbed at $P/P_0 = 0.98$.

Co and Mo contents were obtained by inductively coupled plasma-optical emission spectroscopy (ICP-OES) using an ICPE-9000 spectrometer (Shimadzu, Kyoto, Japan). Typically, 20 mg of each catalyst was added to a digestor with 10 mL of HNO_3 (1:1). After that, the liquid sample was diluted and analyzed.

High angle annular dark field scanning transmission electron microscopy (HAADF-STEM) analyses of some selected catalysts were performed using an FEI Talos F200X microscope (Thermo Fisher Scientific, Hillsboro, OR, USA) operating at 200 kV, equipped with an X-FEG electron source.

3.5. Catalytic Reactions

Reactions were carried out in a 100 mL stainless steel batch reactor (Parr Instruments, Moline, IL, USA, model USA mod HPHT 4598). In a typical run, 500 mg of SO dissolved in 50 mL of *n*-decane and 100 mg of catalyst were loaded into the reactor. The system was purged three times with N_2, followed by three additional purging cycles with H_2. The H_2 pressure was then set to 20 bar at room temperature, and the reactor was heated to 325 °C and maintained at this temperature for 3 h under stirring at 300 rpm. At completion of the reaction, the reactor was rapidly cooled to room temperature, and gaseous and liquid products were collected.

Additional catalytic experiments were also conducted: (a) a blank experiment (no catalyst); (b) a support-only reaction; (c) a physical mixture experiment using Co and Mo monometallic catalysts (100 mg each); and (d) assessment of the best-performing catalyst using WCO as the substrate.

3.6. SO and WCO Characterization

The fatty acid profile of SO was provided by the supplier and determined according to ISO-12966-4 (Animal and vegetable fats and oils—Gas chromatography of fatty acid methyl esters—Part 4: Determination by capillary gas chromatography) [39]. On the other hand, the fatty acid profile of WCO was determined experimentally after transesterification. Briefly, the reaction was carried out using 1.5 g of KOH, 120 mL of CH_3OH, and 200 mL of WCO. Initially, KOH was completely dissolved in methanol at 50 °C. Subsequently, preheated WCO was added, and the mixture was stirred at 800 rpm for 60 min. After completion of the reaction, the mixture was allowed to settle, and the remaining product was separated from the glycerol layer. The resulting fatty acid methyl esters were analyzed by gas chromatography to determine the fatty acid composition. The results are presented in Table S1.

3.7. Analytic Methods

Liquid products (C_7–C_{24} alkanes) were analyzed using a Shimadzu TQ8040-NX (Shimadzu, Kyoto, Japan) gas chromatograph coupled to a mass spectrometer (GC–MS) equipped with a ZB-5MS-Plus (Phenomenex Inc., Torrance, CA, USA) capillary column (30 m × 0.25 mm × 0.25 μm; stationary phase: 5% polysilarylene–95% dimethylpolysiloxane). The GC-MS operating conditions were as follows: split ratio of 20:1, injection volume of 1 μL, oven temperature ramped from 40 °C to 325 °C at 20 °C min^{-1} and held at 325 °C for 15 min, injector temperature of 280 °C, and ion source temperature of 220 °C.

Gaseous products (C_1–C_5 alkanes) were analyzed using a DANI model 1000 (DANI Instruments S.p.A., Monza, Italy) gas chromatograph equipped with a flame ionization detector (GC-FID) and a ValcoPlot Alumina (Valco Instruments Co. Inc., Houston, TX, USA) column (30 m × 0.53 m × 10.0 µm). The operating conditions were: injection volume of 0.5 mL, oven temperature held at 80 °C for 20 min, injector temperature of 250 °C, and FID temperature of 220 °C.

As triglycerides present in SO and WCO cannot be directly identified or quantified by GC-MS, conversion was estimated using Equation (1), where $n_{C_{Oil}}$ represents the total moles of carbon in the oil feed (SO or WCO), calculated from the lipid profile of each oil, and n_{C_i} corresponds to the moles of carbon in each identified compound in the liquid and gaseous products. The selectivity of compound i was calculated according to Equation (2). The iso- to n-alkane ratio in the C_8–C_{16} range (iso/n C_8–C_{16}) was determined using Equation (3).

Selected experiments were conducted in triplicate. The standard deviation associated with conversion was ±4%, while those associated with the selectivity of C_1–C_4, C_5–C_7, C_8–C_{16}, C_{17}–C_{24}, and oxygenated compounds were ±2%, ±1%, ±3%, ±1%, ±1%, and ±4%, respectively. The standard deviation of iso/n (C_8–C_{16}) ratio was ±0.3.

$$Conversion\ (\%) = \frac{\sum n_{C_i}}{n_{C_{Oil}}} \times 100 \quad (1)$$

$$Selectivity_i\ (\%) = \frac{C\ mol\ of\ product\ i}{\sum n_{C_i}} \times 100 \quad (2)$$

$$\frac{\text{iso}}{n}(C_8 - C_{16}) = \frac{mol\ of\ \text{iso}\ C_8 - C_{16}}{mol\ of\ n\ C_8 - C_{16}} \quad (3)$$

4. Conclusions

Bimetallic Co-Mo catalysts supported on a CNT/H-ZSM-5 composite were successfully synthesized and evaluated for the conversion of lipid feedstocks into hydrocarbons in the SAF range. The presence of Mo_2C in the catalysts reduced at 600 °C significantly enhanced the activity of bimetallic catalysts for the conversion of SO into SAF-range hydrocarbons. Increasing the Mo content did not lead to substantial changes in catalytic activity. However, Co loadings below 2.5 wt% were insufficient to achieve effective conversion of SO into SAF-range products.

The best catalytic performance was obtained with a catalyst containing 2.5 wt% Co and 8 wt% Mo, achieving an SO conversion of 82%, a selectivity of 54% toward the C_8–C_{16} fraction, and an iso/n ratio of 2.2. The bimetallic catalyst outperformed both the corresponding monometallic catalysts and their physical mixture, clearly demonstrating a synergistic effect between Co and Mo species.

Finally, the lower conversion and reduced selectivity toward SAF-range hydrocarbons observed for WCO were mainly attributed to the higher complexity and impurity content of this feedstock, highlighting the strong influence of feedstock purity on catalytic performance.

Supplementary Materials: The following supporting information can be downloaded at: https://www.mdpi.com/article/10.3390/catal16050410/s1, References [40,41] are cited in the supplementary materials. Table S1: Fatty acid profiles of SO and WCO. Figure S1. Isotherms of: (A) bimetallic catalysts reduced at different temperatures, (B) bimetallic catalysts with different metal loadings and (C) monometallic catalysts and support.

Author Contributions: K.K.F.: Data curation; formal analysis; methodology; validation; visualization; investigation; writing—original draft; writing—review and editing. L.S.R.: Conceptualization; methodology; supervision; funding acquisition; writing—review and editing. M.F.R.P.: Conceptualization; methodology; supervision; resources; funding acquisition; writing—review and editing. All authors have read and agreed to the published version of the manuscript.

Funding: This work was financially supported by national funds through the FCT/MECI, under the project Waste2Jet—Food Waste Catalytic Valorisation into Eco-Friendly Aviation Fuels: A Pathway for Sustainable Air Transportation with reference 2024.14180.PEX and with DOI https://doi.org/10.54499/2024.14180.PEX. This work was also financially supported by Fundação para a Ciência e a Tecnologia, I.P./MECI through national funds: LSRE-LCM, UID/50020/2025 (https://doi.org/10.54499/UID/50020/2025); and ALiCE, LA/P/0045/2020 (https://doi.org/10.54499/LA/P/0045/2020). K.K. Ferreira acknowledges her Ph.D. scholarship (DOI: 10.54499/2022.12949.BD) from FCT. L.S. Ribeiro and M.F.R. Pereira are members of the CYTED BioFuturo network (424RT0157).

Data Availability Statement: The original contributions presented in this study are included in this article/the Supplementary Materials. Further inquiries can be directed to the corresponding author.

Conflicts of Interest: The authors declare no conflicts of interest.

References

1. Liang, Y.Y.; Shahabuddin, M.; Ahmed, S.F.; Tan, J.X.; Ali, S.M. Optimizing sustainable aviation fuel supply chains: Challenges, mitigation strategies and modeling advances. *Fuel* **2025**, *402*, 135972. [CrossRef]
2. Zubi, G.; Kuhn, M.; Makridis, S.; Coutinho, S.; Dorasamy, S. Aviation sector decarbonization within the hydrogen economy—A UAE case study. *Energy Policy* **2025**, *198*, 114520. [CrossRef]
3. Jiang, C.; Liu, Y. The role of sustainable aviation fuel in CORSIA: An economic analysis. *Energy Econ.* **2025**, *143*, 108238. [CrossRef]
4. Abrantes, I.; Ferreira, A.F.; Silva, A.; Costa, M. Sustainable aviation fuels and imminent technologies—CO_2 emissions evolution towards 2050. *J. Clean. Prod.* **2021**, *313*, 127937. [CrossRef]
5. Zhang, W.; Zhao, Z.; Li, C.; Yang, J.; Qin, Q. Evaluation of sustainable aviation fuel based on life cycle prediction model. *Resour. Conserv. Recycl.* **2026**, *224*, 108565. [CrossRef]
6. Heyne, J.; Rauch, B.; Le Clercq, P.; Colket, M. Sustainable aviation fuel prescreening tools and procedures. *Fuel* **2021**, *290*, 120004. [CrossRef]
7. Zahid, I.; Nazir, M.H.; Chiang, K.; Christo, F.; Ameen, M. Current outlook on sustainable feedstocks and processes for sustainable aviation fuel production. *Curr. Opin. Green Sustain. Chem.* **2024**, *49*, 100959. [CrossRef]
8. Mansy, A.E.; Daniel, S.; Fonzeu Monguen, C.K.; Wang, H.; Osman, A.I.; Tian, Z.Y. Catalytic production of aviation jet biofuels from biomass: A review. *Environ. Chem. Lett.* **2025**, *23*, 419–461. [CrossRef]
9. Lau, J.I.C.; Wang, Y.S.; Ang, T.; Seo, J.C.F.; Khadaroo, S.N.B.A.; Chew, J.J.; Ng Kay Lup, A.; Sunarso, J. Emerging technologies, policies and challenges toward implementing sustainable aviation fuel (SAF). *Biomass Bioenergy* **2024**, *186*, 107277. [CrossRef]
10. Xu, Z.; Shi, W.; Wang, M.; Zhong, S.; Zhou, Y.; Pei, J.; Shao, L.; Pan, K.; Song, Y. Performance and combustion characteristics of Heavy-Fuel aircraft piston engines at high altitudes: Comparison between conventional fuels and HEFA sustainable aviation fuel. *Sustain. Energy Technol. Assess.* **2025**, *75*, 104210. [CrossRef]
11. Yeletsky, P.M.; Kukushkin, R.G.; Yakovlev, V.A.; Chen, B.H. Recent advances in one-stage conversion of lipid-based biomass-derived oils into fuel components—Aromatics and isomerized alkanes. *Fuel* **2020**, *278*, 118255. [CrossRef] [PubMed]
12. Song, M.; Zhang, X.; Chen, Y.; Zhang, Q.; Chen, L.; Liu, J.; Ma, L. Hydroprocessing of lipids: An effective production process for sustainable aviation fuel. *Energy* **2023**, *283*, 129107. [CrossRef]
13. Okolie, J.A.; Awotoye, D.; Tabat, M.E.; Okoye, P.U.; Epelle, E.I.; Ogbaga, C.C.; Gü, F.; Oboirien, B. Multi-criteria decision analysis for the evaluation and screening of sustainable aviation fuel production pathways. *iScience* **2023**, *26*, 106944. [CrossRef]
14. Li, T.; Cheng, J.; Huang, R.; Yang, W.; Zhou, J.; Cen, K. Hydrocracking of palm oil to jet biofuel over different zeolites. *Int. J. Hydrogen Energy* **2016**, *41*, 21883–21887. [CrossRef]
15. de Sousa, F.P.; Pasa, V.M.D. Catalytic deoxygenation of palm oils to produce bio-hydrocarbons in the range of sustainable aviation fuels (SAF) and green diesel over Nb_2O_5. *Mol. Catal.* **2025**, *585*, 115354. [CrossRef]
16. Saviola, A.J.; Wijaya, K.; Fitria, R.A.; Chang, S.W.; Ravindran, B.; Amin, A.K.; Fitria, A.; Syoufian, A. Unlocking the potential of converting non-edible oils into sustainable jet fuel-range hydrocarbons using simply prepared nickel- or molybdenum-promoted zirconia catalysts. *Sustain. Chem. Clim. Action* **2025**, *7*, 100126. [CrossRef]

17. Nugroho, A.; Candra Dewi, P.D.; Sudiyarmanto; Hidayati, L.N.; Kristiani, A.; Aulia, F.; Bakti, A.N.; Prasetyo, J.; Rinaldi, N.; Dahnum, D. Catalytic deoxygenation of coconut oil to bio-jet fuel range hydrocarbon over nickel on ZIF-67-derived metal oxide. *Fuel* **2026**, *407*, 137430. [CrossRef]
18. Tanwongwan, W.; Sartsamai, R.; Kaewmeesri, R.; Faungnawakij, K.; Chollacoop, N.; Assabumrungrat, S.; Fuji, M.; Eiad-Ua, A. Potential of advanced microporous zeolites and mesoporous materials derived from natural precursors as supports for iron phosphide catalysts in bio-jet fuel production from palm oil (*Elaeis guineensis*). *RSC Adv.* **2025**, *15*, 19714–19725. [CrossRef] [PubMed]
19. Ahmad, J.; Chotirattanachote, A.; Sedtabute, S.; Rashid, U.; Ngamcharussrivichai, C. Hydrogen-free catalytic hydrothermolysis of palm oil into sustainable aviation fuel-range hydrocarbons over Ni/AC–Al_2O_3 catalysts. *Process Saf. Environ. Prot.* **2025**, *204*, 108139. [CrossRef]
20. Castillo Monroy, E.F.; García Pérez, M.; Vásquez Carrillo, M.C.; Martinez Valencia, L.; Martínez Gonzalez, A. Aviation fuels, vegetable oil hydrotreating, and drop-in fuels. In *From Crops and Wastes to Bioenergy: Current Status and Challenges*; Elsevier: Amsterdam, The Netherlands, 2025; pp. 585–631. [CrossRef]
21. Mäki-Arvela, P.; Martínez-Klimov, M.; Murzin, D.Y. Hydroconversion of fatty acids and vegetable oils for production of jet fuels. *Fuel* **2021**, *306*, 121673. [CrossRef]
22. Wei, L.; Wang, H.; Dong, Q.; Li, Y.; Xiang, H. A Review on the Research Progress of Zeolite Catalysts for Heavy Oil Cracking. *Catalysts* **2025**, *15*, 401. [CrossRef]
23. Hammond, C.; Padovan, D.; Tarantino, G. Porous metallosilicates for heterogeneous, liquid-phase catalysis: Perspectives and pertaining challenges. *R. Soc. Open Sci.* **2018**, *5*, 171315. [CrossRef] [PubMed]
24. Cheah, K.W.; Yusup, S.; Loy, A.C.M.; How, B.S.; Skoulou, V.; Taylor, M.J. Recent advances in the catalytic deoxygenation of plant oils and prototypical fatty acid models compounds: Catalysis, process, and kinetics. *Mol. Catal.* **2022**, *523*, 111469. [CrossRef]
25. Pérez-Mayoral, E.; Calvino-Casilda, V.; Soriano, E. Metal-supported carbon-based materials: Opportunities and challenges in the synthesis of valuable products. *Catal. Sci. Technol.* **2016**, *6*, 1265–1291. [CrossRef]
26. Duan, P.; Wang, B.; Xu, Y. Catalytic hydrothermal upgrading of crude bio-oils produced from different thermo-chemical conversion routes of microalgae. *Bioresour. Technol.* **2015**, *186*, 58–66. [CrossRef] [PubMed]
27. Ferreira, K.K.; Di Stasi, C.; Ayala-Cortés, A.; Ribeiro, L.S.; Pinilla, J.L.; Suelves, I.; Pereira, M.F.R. Hydroprocessing of waste cooking oil to produce liquid fuels over Ni-Mo and Co-Mo supported on carbon nanotubes. *Biomass Bioenergy* **2024**, *191*, 107480. [CrossRef]
28. Ding, R.; Wu, Y.; Chen, Y.; Chen, H.; Wang, J.; Shi, Y.; Yang, M. Catalytic hydrodeoxygenation of palmitic acid over a bifunctional Co-doped MoO_2/CNTs catalyst: An insight into the promoting effect of cobalt. *Catal. Sci. Technol.* **2016**, *6*, 2065–2076. [CrossRef]
29. Ferreira, K.K.; Ribeiro, L.S.; Pereira, M.F.R. Analysis of Reaction Conditions in Palmitic Acid Deoxygenation for Fuel Production. *Catalysts* **2024**, *14*, 853. [CrossRef]
30. Ribeiro, L.S.; Di Stasi, C.; Ayala-Cortés, A.; Ferreira, K.K.; Pinilla, J.L.; Suelves, I.; Pereira, M.F.R. From waste to fuel: Catalytic conversion of waste cooking oil in batch and continuous modes. *Bioresour. Technol.* **2026**, *442*, 133659. [CrossRef]
31. Ferreira, K.K.; Magalhães, B.F.O.; Ribeiro, L.S.; Pereira, M.F.R. Co–Mo Catalysts Supported on CNT/H-ZSM-5 Composites for Selective Production of Sustainable Aviation Fuel-Range Alkanes. *Energy Fuels* **2025**, *39*, 14615–14626. [CrossRef]
32. Gu, W.; Xing, M.; Chen, J.; Li, L.; Peng, Z.; Sun, M.; Xie, J.; Tang, J.; Chen, M.; Chen, B.; et al. Hydrodeoxygenation of cottonseed oil to alkanes using effective and stable Mo-Ni-based bifunctional catalysts with optimized support. *J. Catal.* **2026**, *454*, 116648. [CrossRef]
33. Muñoz-Arjona, A.; Ayala-Cortés, A.; Di Stasi, C.; Torres, D.; Pinilla, J.L.; Suelves, I. Catalytic hydrodeoxygenation of waste cooking oil into green diesel range hydrocarbons: From batch to continuous processing. *Chem. Eng. J.* **2025**, *503*, 158303. [CrossRef]
34. Wang, L.; Sun, B.H.; Yu, J.J.; Li, J.L. A new method for preparing ultrafine Mo_2C by the CVD reaction of CO and gaseous MoO_3: Parameter optimization and its formation mechanism. *Int. J. Refract. Met. Hard Mater.* **2026**, *136*, 107636. [CrossRef]
35. Cárdenas, J.; Orjuela, A.; Sánchez, D.L.; Narváez, P.C.; Katryniok, B.; Clark, J. Pre-treatment of used cooking oils for the production of green chemicals: A review. *J. Clean. Prod.* **2021**, *289*, 125129. [CrossRef]
36. Romero, D.; Rigutto, M.; Hensen, E.J.M. Mechanistic aspects of n-hexadecane hydroconversion: Impact of di-branched isomers on the cracked products distribution. *Fuel* **2024**, *358*, 130264. [CrossRef]
37. Sun, J.; Mu, C.; Guo, D.; Zhao, Y.; Wang, S.; Ma, X. Effects of Intimacy between Acid and Metal Sites on the Isomerization of n-C16 at the Large/Minor Nanoscale and Atomic Scale. *ACS Catal.* **2022**, *12*, 4092–4102. [CrossRef]
38. Verma, V.; Mishra, A.; Anand, M.; Farooqui, S.A.; Sinha, A.K. Catalytic hydroprocessing of waste cooking oil for the production of drop-in aviation fuel and optimization for improving jet biofuel quality in a fixed bed reactor. *Fuel* **2023**, *333*, 126348. [CrossRef]
39. *ISO 12966-4:2015*; Animal and Vegetable Fats and Oils—Gas Chromatography of Fatty Acid Methyl Esters Part 4: Determination by Capillary Gas Chromatography. International Organization for Standardization: Geneva, Switzerland, 2015.

40. Aviludo–Óleo Fula de girasol. Available online: https://www.aviludo.pt/pt/ful/oleo-fula-girassol-6x3-l_p4018.html?id=36&cat=0&pc=1 (accessed on 17 December 2025).
41. Muñoz-Arjona, A.; Torres, D.; Di Stasi, C.; Suelves, I.; Pinilla, J.L. Instituto de Carboquímica, CSIC: Zaragoza, Spain. 2026, *manuscript under preparation*.

Disclaimer/Publisher's Note: The statements, opinions and data contained in all publications are solely those of the individual author(s) and contributor(s) and not of MDPI and/or the editor(s). MDPI and/or the editor(s) disclaim responsibility for any injury to people or property resulting from any ideas, methods, instructions or products referred to in the content.